



This is a repository copy of *Evolution of electroplated cBN tool surface texture parameters during point grinding*.

White Rose Research Online URL for this paper:

<https://eprints.whiterose.ac.uk/188618/>

Version: Published Version

Article:

Pietrow, N., Curtis, D., Novovic, D. et al. (2 more authors) (2022) Evolution of electroplated cBN tool surface texture parameters during point grinding. *Journal of Manufacturing Science and Engineering*, 144 (12). 121007. ISSN 1087-1357

<https://doi.org/10.1115/1.4054990>

Reuse

This article is distributed under the terms of the Creative Commons Attribution (CC BY) licence. This licence allows you to distribute, remix, tweak, and build upon the work, even commercially, as long as you credit the authors for the original work. More information and the full terms of the licence here:

<https://creativecommons.org/licenses/>

Takedown

If you consider content in White Rose Research Online to be in breach of UK law, please notify us by emailing eprints@whiterose.ac.uk including the URL of the record and the reason for the withdrawal request.



eprints@whiterose.ac.uk
<https://eprints.whiterose.ac.uk/>

Nikita Pietrow¹

Industrial Doctorate Centre in Machining Science,
Advanced Manufacturing Research Centre,
University of Sheffield,
Rotherham S60 5TZ, UK;
Department of Mechanical Engineering,
University of Sheffield,
Sheffield S1 3JD, UK
e-mail: npietrow1@gmail.com

David Curtis

Advanced Manufacturing Research Centre,
University of Sheffield,
Catcliffe, Rotherham S60 5TZ, UK
e-mail: d.curtis@amrc.co.uk

Donka Novovic

Rolls-Royce plc.,
Derby DE24 8BJ, UK
e-mail: donka.novovic@rolls-royce.com

Jamie McGourlay

Rolls-Royce plc.,
Derby DE24 8BJ, UK
e-mail: jamie.mcgourlay@rolls-royce.com

Hassan Ghadbeigi

Department of Mechanical Engineering,
University of Sheffield,
Sheffield S1 3JD, UK
e-mail: h.ghadbeigi@sheffield.ac.uk

Evolution of Electroplated Cubic Boron Nitride Tool Surface Texture Parameters During Point Grinding

Point grinding is an abrasive machining process that utilizes small diameter superabrasive single-layer grinding tools for accurate machining of complex 3D geometries. Due to the small nature of these tools, high wear-rates and uneven wear around the tool circumference present a challenge for their successful application for the finish machining of metallic components. It is, therefore, essential to monitor the surface condition of the point grinding tools, to ensure their safe and reliable operation. In this investigation, the 3D topography evolution of single-layer B126 cubic boron nitride (cBN) point grinding tools was characterized using focus-variation imaging. Given the wealth of information obtained using this method, a decision-matrix methodology was used to identify the most important parameters for monitoring the wear condition of the point grinding tools. Grinding trials were also performed with fixed cutting parameters and varied cutting durations up to 520 mm³ of material removed to assess the evolution of the point grinding tool surfaces over time as a result of wear during grinding of hardened D2 tool steel. The best criteria for the characterization of the surface texture of electroplated cBN point grinding tool surfaces were identified to be the average surface height (Sa), skewness (Ssk), root mean square gradient (Sdq), reduced peak height (Spk), peak material volume (Vmp), and developed interfacial area ratio (Sdr). These parameters performed best for direct measurement of point grinding tool surfaces, paving the way for the application of the imaging technique under manufacturing conditions as an on-machine monitoring method for performance assessment.

[DOI: 10.1115/1.4054990]

Keywords: grinding and abrasive processes, machining processes, point grinding, metrology

1 Introduction

Grinding is a material removal process that utilizes hard abrasive grains as a cutting medium. It is mainly applied as a finish machining operation for components that require a high-quality surface finish, fine tolerances and general machining of difficult-to-cut materials. There are many types of grinding operations with varying grinding wheel shapes and kinematics of the process [1]. The type of grinding wheels used, utilizing conventional Al₂O₃ or SiC abrasives, or superabrasive diamond and cubic boron nitride (cBN) grains in either vitrified, resin, or metallic bonds, can also vary depending on the process and the machined component requirements. With superabrasive grinding wheels, in particular, a single-layer configuration is often used, where only a single-layer of abrasive grains exists on the wheel's surface. The use of such single-layer superabrasive wheels presents several advantages over their conventional counterparts, including good form retention over long grinding times, no wheel preparation requirement such as dressing, re-use of the wheel after severe wear through reapplication of the grains, and a higher relative spacing between the grains that helps reduce the grinding temperature and enables the use of higher removal rates [2,3].

When attempting to abrasively machine small or complex components, conventional grinding can often struggle due to the large and inflexible size of the grinding wheel used. In such instances, the use of small-scale point grinding tools is necessary. Point grinding is an

abrasive machining process that utilizes small diameter superabrasive single-layer grinding tools for accurate machining of complex 3D geometries. The significant reduction in the size of the point grinding tools from that of conventional 100–300 mm grinding diameter to sub 15 mm diameter brings about the main advantage of the process: the ability to machine small or difficult to access complex features where conventional grinding is not suitable. In addition, the use of point grinding tools can also help improve the overall flexibility of the grinding operation when utilized together with high-speed tool-changeable attachment spindles, such as the one applied in this investigation. This allows point grinding to be integrated with other machining processes, removing the need for large grinding machines and potentially displacing less flexible operations [4,5]. However, alongside the advantages, the small diameter of the tools also brings about several challenges.

As was reported earlier, numerous issues must be resolved for the successful application of point grinding tools for machining hardened metallic components, including critical aspects such as high wear-rates and variation in the condition of the abrasive grains on the surface of the tools [6]. In general, the single-layer configuration limits the efficient grinding life of superabrasive wheels due to the low number of grains present on the surface [7], and this issue becomes even more significant for point grinding tools due to their small diameter as the number of abrasive grains is further reduced. When combined with the relatively high wear-rates and variation in the condition of the grains, rapid degradation of the tool surface during point grinding can occur, resulting in low overall tool life compared to their conventionally sized counterparts. This makes the continuous monitoring of these tools necessary to ensure safe operation and reliable performance.

¹Corresponding author.

Manuscript received November 30, 2021; final manuscript received June 24, 2022; published online August 25, 2022. Assoc. Editor: Radu Pavel.

Understanding the wear behavior of the abrasive grains on the surface of single-layer point grinding tools is critically important to optimize their performance, as only a limited number of grains exist on the surface of the tools. This area has, therefore, attracted significant attention within the research community. Electroplated cBN tools have been shown to wear by three main mechanisms, including attrition, grain fracture, and grain pullout [7–9]. Rapid wear through grain pullout occurs during the early stages of grinding and, as the name suggests, involves the complete removal of the abrasive grain from the tool's surface. The fracturing of the abrasive grains can also occur, removing large portions of the grain and leaving behind a rough irregular surface, or rough wear flats in the case of micro fracturing [7]. Following the initial transient wear, where pullout and fracturing dominate, steady-state wear evolution is reached, during which attritious wear causes dulling of the abrasive grain tips and formation of smooth wear flats along with striation marks in the grinding direction, and progressively increasing number of active grains as the most protruding grains wear down [7,10]. It is reported that the wear behavior of electroplated cBN grains is highly dependent on the properties of the abrasive grade, workpiece material, and process parameters with variations in the observed active mechanisms commonly observed, such as a reduced tendency for pullout [11] or reduced fracturing in some cases [12]. However, a common feature across all earlier work is the conclusion that the surface topography of the grinding wheel changes dramatically as a result of wear [7].

It is also known that the kinematic interactions between the grains and workpiece material are affected by the topography of the grinding wheel surface with a profound effect on the grinding forces, power, temperature, and surface finish of components [13]. Several tactile (e.g., profilometry or imprints methods) and non-contact (e.g., laser triangulation and interferometry) techniques have already been used to monitor and quantify the grinding wheel's topography. Non-contact techniques are a more common practice, as contact-based measurements present a challenge due to the wear of the measuring device [14–16]. Therefore, optical full-field measurements using focus-variation microscopy provide an appropriate method for non-destructive characterization of 3D topography of grinding wheels. However, given the wealth of information obtained from these methods, selecting the most representative and reliable surface texture parameters for assessing the wheel condition is vital for understanding its performance.

In this context, as many as 144 surface texture parameters have previously been considered for assessing grinding wheels' condition [11]. These could be categorized into three groups of surface texture parameters, including height-based, hybrid, and functional parameters [11,17–19] presented in Table 1 according to ISO 25178 [20]. Since most of these are linked to similar surface properties, (e.g., maximum heights: Sz and S10z), such a large number of parameters is unnecessary and impractical for monitoring the condition of grinding wheels.

Barth and Klocke [17] showed that the surface's hybrid Sdr and Sdq values and functional Spk and Vmp parameters correlate highly

with measured grinding forces and temperature in resin bonded cBN grinding wheels when comparing new and worn wheels. Similarly, Bazan et al. [11] reported that Vmp correlates highly with the wear of electroplated cBN wheels, while Spk has been used in the past to quantify the wear of electroplated cBN point grinding tools [12]. Additionally, from the set of height-based parameters, Sq, Ssk, and Sku performed well for grinding wheel condition monitoring but generally correlated to a lesser extent than hybrid and functional parameters [11,18]. While similarities in the earlier investigations into the measurement of various grinding wheel's surface textures could be seen, there is a gap in the knowledge concerning the selection of the most useful parameters for monitoring the condition of point grinding tools, where higher wear-rates and varying wear mechanisms can be expected. It is also unknown how the various surface texture parameters evolve with wear throughout the tool life, as earlier works focused only on fixed grinding durations and varied cutting parameters [11,17,18]. Therefore, the present research aims to identify the most significant parameters for monitoring the condition of single-layer cBN point grinding tools using a decision-matrix methodology and assess their evolution over time due to wear. Direct optical surface measurements of the electroplated cBN tool surfaces, without the creation of replicas, will also be used to simulate and account for the imaging errors and practical challenges associated with the application of the imaging technique as an on-machine monitoring method under manufacturing conditions.

2 Experimental Methodology

In order to assess the evolution of the tool surfaces with wear throughout their total life and identify the most significant surface texture parameters that relate to their condition, an assessment of the point grinding tools before and after grinding for the varied cutting duration was required. Therefore, grinding trials were designed utilizing small diameter single-layer cBN point grinding tools of a 6 mm diameter performed on a five-axis Makino G7i horizontal machining center. A through-tool coolant-driven attachment spindle (Colibri TJS HPC), capable of achieving rotational speeds of up to 42,000 rpm, was also used to achieve the highest possible cutting speeds, which was necessary due to the small diameter of the tools. The material used for this investigation consisted of thin plates (77 × 40 × 3 mm) of D2 tool steel, hardened to 60HRC and secured using a custom steel fixture. TRIM C272 (9%) coolant was supplied at 70 bar through the attachment spindle to rotate the tool and 30 bar through the external nozzle simultaneously. The external coolant nozzle was positioned at a high stand-off distance of 100 mm to reduce the unwanted high tool deflecting forces introduced into the system while still providing sufficient tool cooling and chip evacuation. The grinding forces were recorded using a Kistler (Type 9129AA) multi-component dynamometer at a sampling rate of 50 kHz. An overview of the setup used can be seen in Fig. 1(a).

Table 1 Commonly used standard surface texture parameters (ISO 25178)

Height-based and hybrid texture parameters			Functional texture parameters		
Name	Unit	Description	Name	Unit	Description
Sa	μm	Average height	Sk	μm	Core roughness depth
Sq	μm	Root mean square height	Spk	μm	Reduced peak height
Sp	μm	Maximum peak height	Svk	μm	Reduced valley height
Sv	μm	Maximum valley depth	Smr1	%	Peak material component
Sz	μm	Maximum height	Smr2	%	Peak material component
S10z	μm	Ten-point height	Vmp	ml/m^2	Peak material volume
Ssk	—	Skewness	Vmc	ml/m^2	Core material volume
Sku	—	Kurtosis	Vvc	ml/m^2	Core void volume
Sdq	—	Root mean square gradient	Vvv	ml/m^2	Valley void volume
Sdr	%	Developed interfacial area ratio			

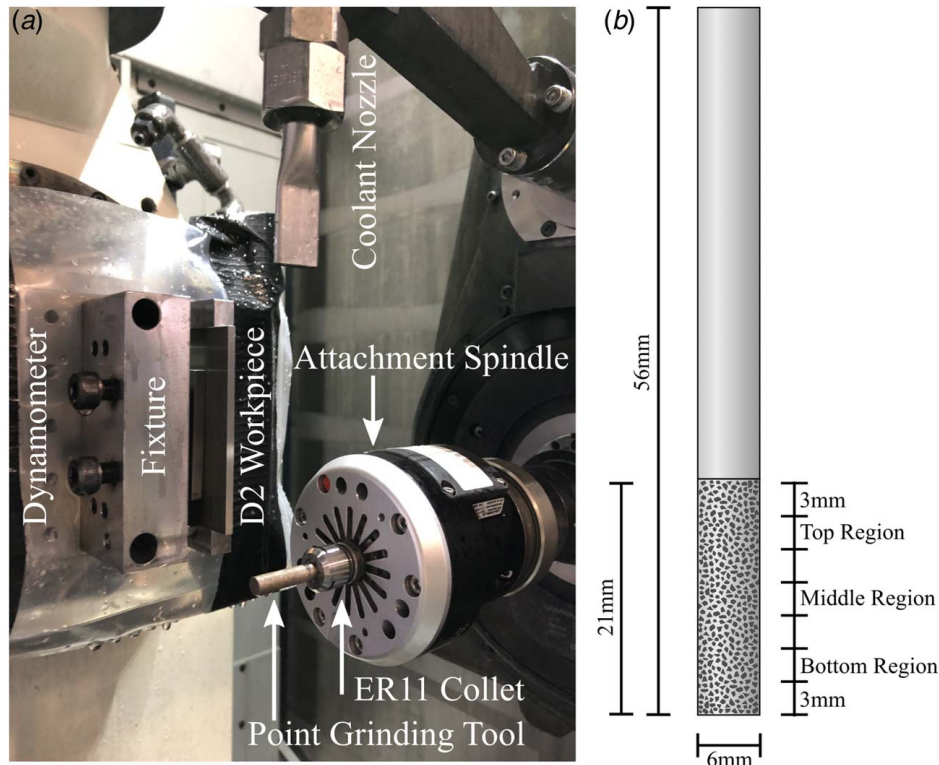


Fig. 1 (a) Grinding setup and (b) schematic representation of the point grinding tool and three grinding positions utilized in this investigation

Figure 1(b) shows a schematic of point grinding tools used in this study. The tool body was manufactured from M42 high-speed steel by centerless grinding to achieve a sub $3\ \mu\text{m}$ total runout followed by a nickel electroplating process to bond the superabrasive cBN grains to the surface of the tool. Two different cBN abrasive grades of ABN300R and ABN800 with a similar nominal grain size of $126\ \mu\text{m}$ were used to assess the impact of abrasive particle properties on the point grinding process. Both abrasive grain products had the same nominal grain size of $126\ \mu\text{m}$. However, the different chemistry reflected in the color of the grains, and manufacturing method employed in the grains' production, resulted in variation in the morphology and relative strength of the abrasive. The color, shape, and strength parameters for classifying abrasive grains are commonly used by manufacturers to describe the various cBN products (Table 2).

Table 3 shows the applied cutting parameters and experimental methodology implemented for the grinding trials using both the abrasive grades, with the duration of the grinding tests being the primary variable to observe the evolution of tool surface texture through different stages of wear. The bottom region of the tool was used for shorter grinding durations to minimize the effect of tool deflections on the grinding performance, while prolonged trials were conducted with the top region of the tool engaging with the workpiece (Fig. 1(b)). The grinding forces were recorded for every cut while the surface textures of the abrasive cutting

regions were assessed before and after the grinding trials, as discussed next.

In order to characterize the evolution of the tool surface, three-dimensional scans of each tool were obtained before and after the specified grinding duration (Table 3) from three sides around the periphery of each tool (Fig. 2). The scans were captured using a $10\times$ objective lens on an Alicona InfiniteFocusSL variable focus microscope. In order to allow for direct comparison of the 3D image fields before and after grinding, a fine locating scratch was created on each side of the tool body before initial tool imaging to act as a reference point for all further imaging, ensuring that exactly the same region was assessed. The total imaged area covered approximately 32% of the total active grinding region around the tool circumference for each cutting position. It is important to note that a different tool surface is used for each test, contributing to some error in the observed trends but resulting in a less biased assessment that is more representative of average tool surfaces.

Due to the small diameter of the tools, a very noticeable curvature could be seen on the resultant image fields, which would significantly impact the measured surface texture properties. Therefore, a Gaussian linear planar second-order filter for arbitrary surfaces (ISO 16610-71 [21]) was applied to all captured image fields to remove this tool curvature while preserving the grain shapes. This filter

Table 2 Unbonded abrasive grains properties

Abrasive	Size (μm)	Color	Average shape	Strength (normalized)
ABN300	126	Amber	Irregular	47
ABN800	126	Brown	Truncated Tetrahedral	100

Table 3 Fixed cutting parameters (top) and variable cutting durations at three positions on the tool surface (bottom)

Grinding parameters	$a = 0.015\ \text{mm}$		$v_s = 13.86\ \text{m/s}$		$v_w = 700\ \text{mm/min}$	
	Tool #1	Tool #2	Tool #3	Tool #4	Tool #5	Tool #6
Varied grinding durations (# passes)						
Top region	52	52	52	100	125	150
Middle region	7	10	30	7	10	30
Bottom region	1	2	4	1	2	4

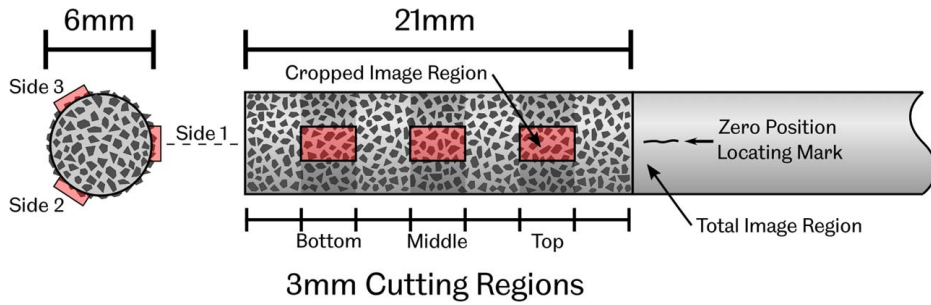


Fig. 2 Alicona imaging locations highlighted across three positions on each side of the point grinding tool. Nine scans were obtained for each point grinding tool, with three for each respective test condition.

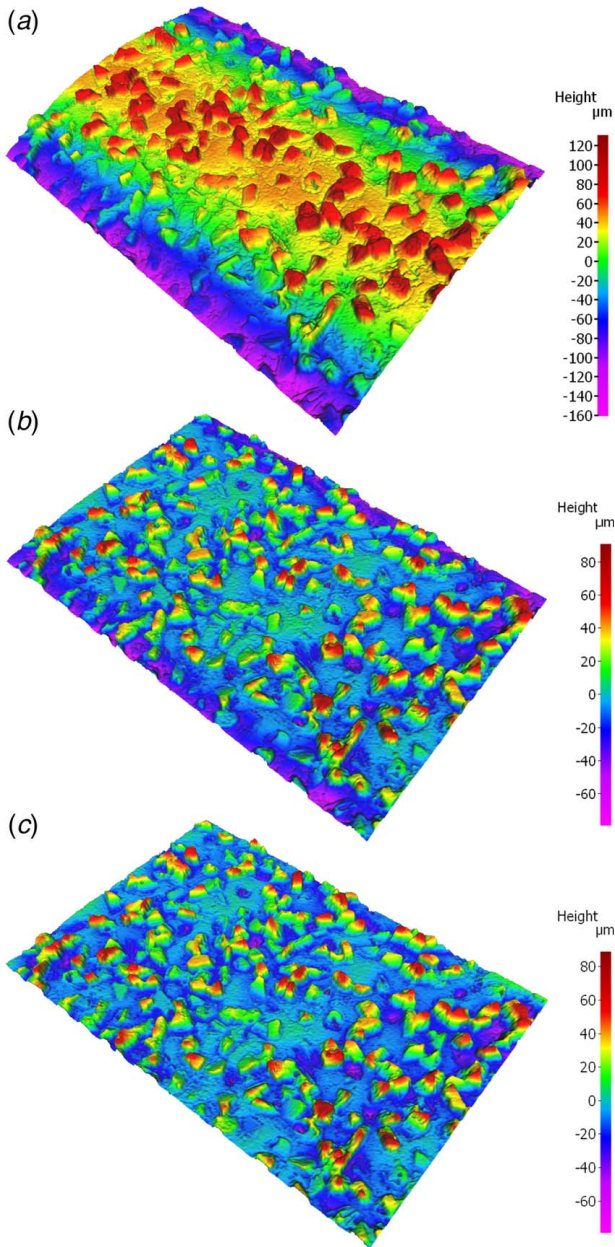


Fig. 3 Example point grinding tool surface image field with visible curvature: (a) before filtering, (b) minor curvature remaining after Gaussian linear planar zero-order filtering, and (c) no curvature after second-order filtering

was selected due to significantly better performance at removing tool curvature around the edges of each image field compared to other filtering options (Fig. 3) and is recommended for surfaces that contain deep valleys and high peaks [21]. Figure 3 shows an example point grinding tool surface before (Fig. 3(a)) and after this filtering was applied (Fig. 3(c)). Following filtering, surface texture parameters listed in Table 1 previously were calculated for each region in new and worn conditions to evaluate the change in the parameters throughout the tool life and identify the best performing parameters for on-machine monitoring of the tool condition.

3 Results

3.1 Grinding Force Evolution. The average normal grinding forces per pass, following subtraction of coolant forces and exclusion of entry and exit forces, have been recorded, and the resultant evolution with the corresponding standard errors is shown in Fig. 4. Following an initial transient increase, the average forces increase steadily following a similar two-stage pattern as previously reported [7,8]. There appears to be almost no difference in the magnitude of the average normal forces between the two abrasive grades; however, the transition from the rapid wear to the steady-state wear region for ABN300 occurs slightly later than ABN800. The estimated transition points at the tested cutting conditions for both abrasives are 34.65 mm^3 and 45.05 mm^3 and marked as A and B, respectively. It is important to note that for longer test durations, fewer repeats were carried out, as shown in Table 3, which resulted

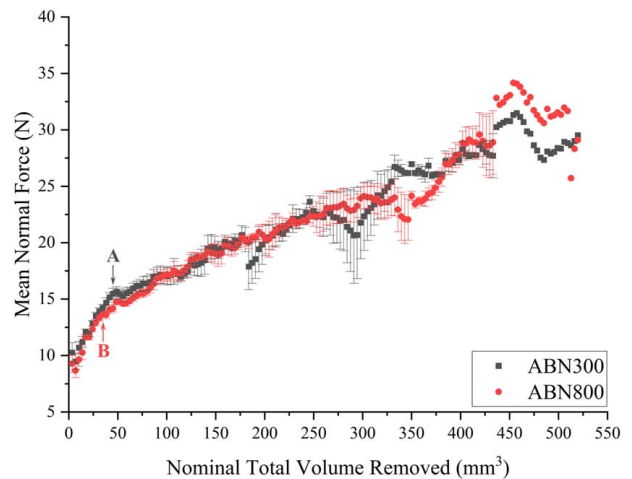


Fig. 4 Evolution of the normal grinding forces during point grinding, including standard errors. Estimated steady-state transition points are marked.

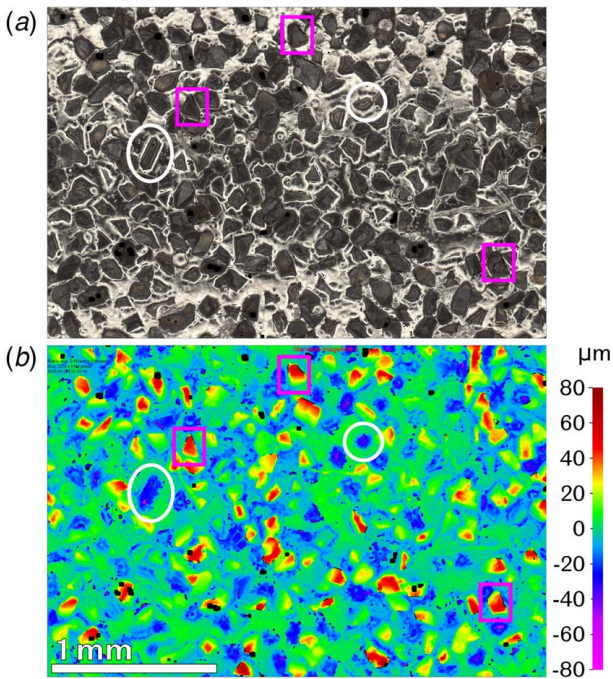


Fig. 5 (a) Example point grinding tool surface optical image and (b) 3D topography data, showing a few highly protruding abrasive grains (boxed) and non-protruding or submerged grains (circled)

in visibly increasing error toward the end of the tests as could be expected.

3.2 Tool Surface Topography. Figure 5 shows representative optical (a) and 3D (b) focus-variation images of an example point grinding tool containing cBN grains protruding above the Nickel bond layer. The stochastic nature of the grains themselves and their ranging protrusion heights are shown and are typical for

single-layer superabrasive grinding tools. While some grains are highly protruding (boxes on figure), a large fraction of the grains are very low, and completely submerged or barely protruding above the bond (circled). Also visible are the black regions in the height map of Fig. 5(b), which are missing data points that result from the highly reflective bond layer and partially transparent nature of the abrasive grains. These were not artificially filled to avoid introducing anomalous features. However, imaging was repeated in severe cases to ensure the quantity of missing data never exceeded 3% of the total observed surface area.

Figure 6 shows the evolution of representative point grinding tool surfaces from the as-received condition until 520 mm^3 of material removed. The average height of the tool surface appears to reduce with increasing test duration, with a notable loss of highly protruding grains tips (reduced number of highly protruding red grain tips). While less obvious, it is also possible to observe a variation of the average surface height around different sides of the same tool, which is later highlighted by the measurement of the texture parameters. This behavior becomes especially noticeable around 34 mm^3 of material removed (Fig. 6) and eventually returns to normal during longer cutting durations. Additionally, around 346.50 mm^3 of material removed, bond engagement was first observed for both abrasive grades (marked in Fig. 6). Initially appeared as small regions of scratches in the cutting direction on the bond material, followed by complete engagement of the bond at the end of the test, it is visible as vertical striation marks. Micrographs of Fig. 7 show these image regions in more detail, confirming that bond engagement had occurred. This visual assessment of the tool surface condition was supported by the measurement of surface texture parameters.

3.3 Evolution of Height-Based and Hybrid Surface Texture Parameters.

Figure 8 shows the evolution of the Sa parameter with the total volume of removed material for both abrasive grains in the form of the average value across repeated tests and corresponding standard errors. During the very first grinding pass, the Sa value for both ABN300 and ABN800 can be seen dropping rapidly. While the average surface height of starting condition for ABN800 tools was around $2 \mu\text{m}$ higher than ABN300, during the early stages of grinding up to 100 mm^3 , both abrasive grades

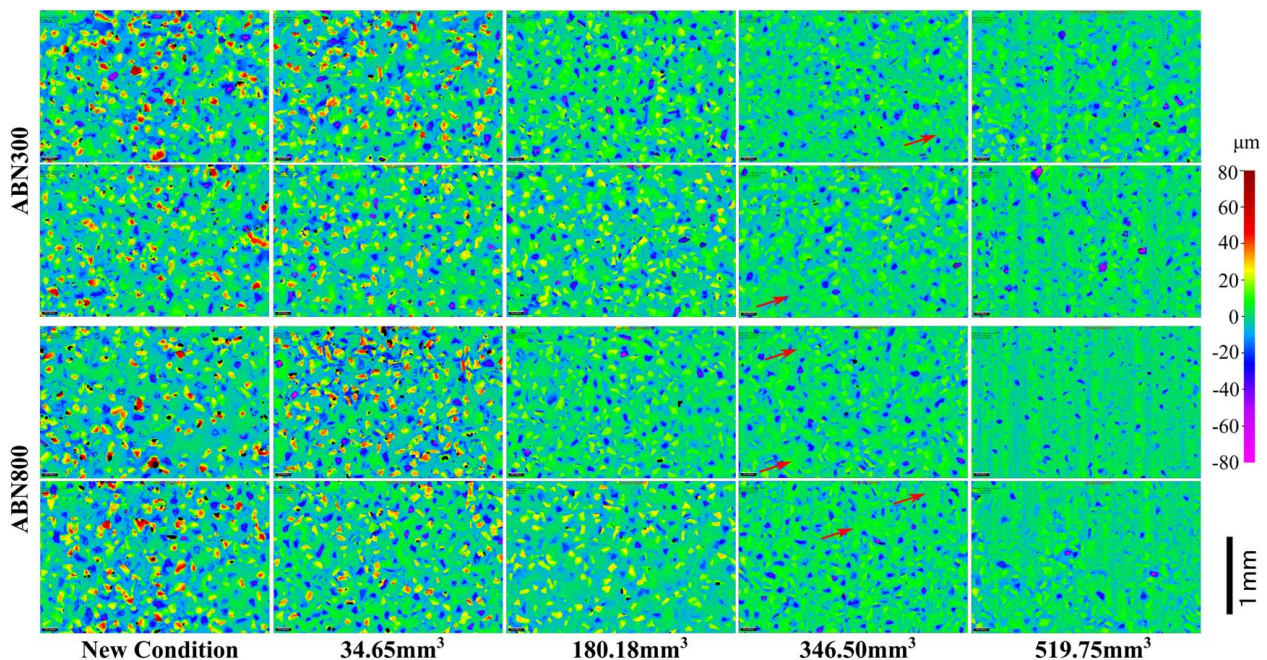


Fig. 6 Evolution of average point grinding tool surfaces with increased volume of material removed. Initial areas of bond engagement are marked with arrows before becoming easily visible as vertical striation marks after 519.75 mm^3 of material was removed.

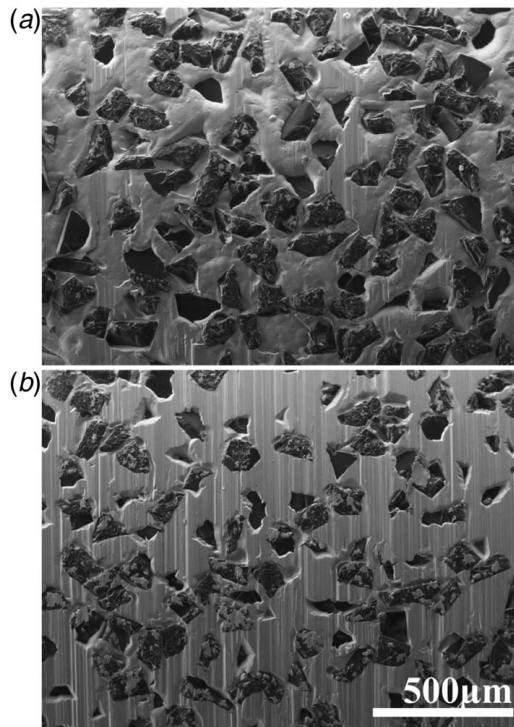


Fig. 7 Secondary electron SEM image of worn ABN800 tool surfaces after (a) 346.50 mm³ and (b) 519.75 mm³ of material removed. Bond wear is visible as vertical scratches in the cutting direction.

behaved similarly, with an initial fast decrease in the overall height of the surface followed by a steady decline with increased test duration. However, the slightly higher rate of decline in the ABN800 abrasive grain height can be seen, eventually reaching almost identical surface height values as ABN300 during the steady-state wear region between 180 mm³ and 340 mm³ material removed. Towards the end of the grinding test, after 346.5 mm³ volume of material

removed where bond engagement occurs, there appeared to be a deviation in the behavior of the two abrasive grades, with ABN 300 leveling out while ABN800 continued to decrease. However, in both cases, the Sa value did not reach 0 even after the most prolonged cutting (519.75 mm³).

Figure 9 shows the evolution of additional height-based parameters, including Sq (root mean square height), Sp (maximum peak height), Sz (maximum height), and S10z (ten-point height) with grinding duration. The starting condition of ABN800 tools was again higher than ABN300 in each case, and the overall observed trend for these parameters was similar to the Sa evolution with an initial rapid drop during the first four grinding passes, followed by a steady decrease until the end of the test. Unlike Sa, however, the observed standard errors between the repeated test were higher for these four parameters, especially towards longer grinding durations (after 346.5 mm³) where fewer repeats are carried out, and in addition, occasional random spikes in the measurements can be seen (e.g., Sz at 346.5 mm³).

Unlike the previously discussed height parameters that measured the surface directly, skewness and kurtosis (Ssk and Sku, respectively) focus on the distribution of the surface heights around the mean value (Fig. 10). Thus, as the tool surface wears, the skewness value (Ssk) is seen to change shape from a skew towards positive values (Ssk > 0) through symmetrical shape (Ssk = 0), and finally reversing the skew towards negative values (Ssk < 0). This behavior is summarized by the plot in Fig. 10(a), where the almost linear evolution of the average Ssk values during point grinding can be seen.

The evolution of the tool surface kurtosis (Sku) showed the most distinct trend compared to all other investigated surface texture parameters and is shown in Fig. 10(b). For both abrasive grades, the Sku values appeared to slowly decline until reaching a minimum value after approximately 103.95 mm³ of material removed. This slow decline was next followed by an exponential spike, with exceptionally high values for ABN300.

The observed trends in the evolution of the surface Sdr and Sdq are presented in Figs. 11(a) and 11(b), respectively, showing identical results. After a significant drop during the first grinding pass, there appeared to be a minor increase in the measured values up to a peak of around 34.65 mm³ of material removed. This early peak was then followed by a steady decrease in both the Sdr and

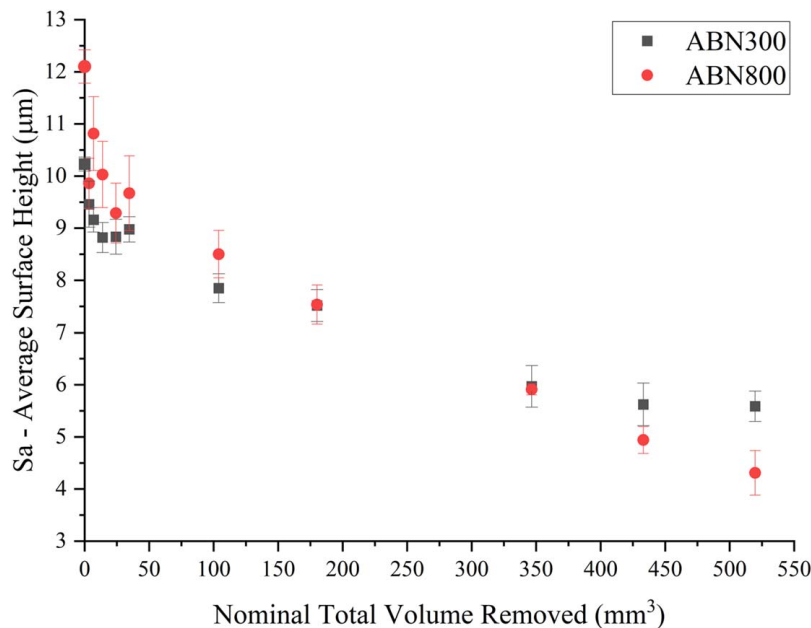


Fig. 8 Evolution of average surface height (Sa) during point grinding. The standard error of the mean is indicated as the error bars.

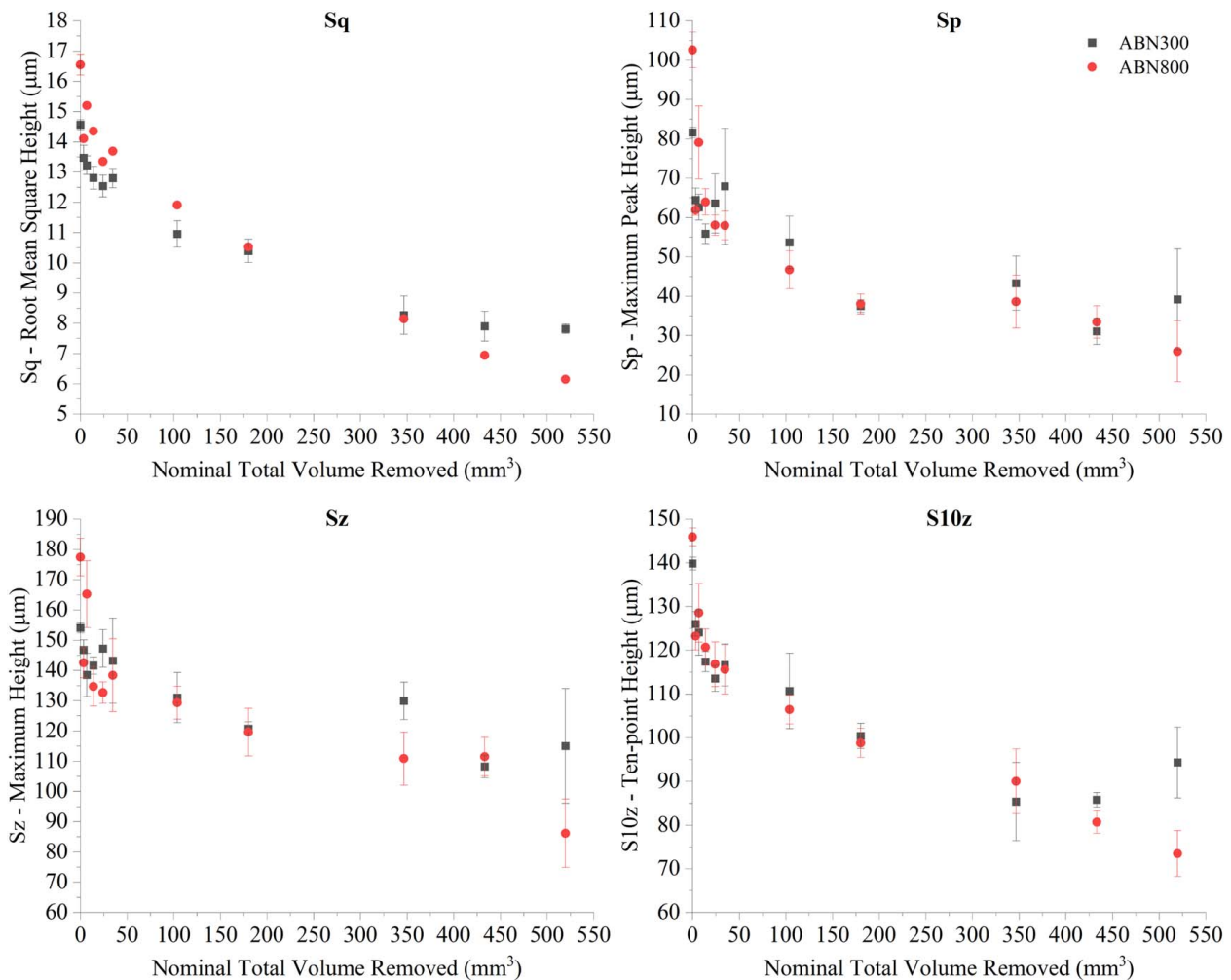


Fig. 9 Evolution of additional height-based parameters (Sq, Sp, Sz, and S10z) during point grinding. The standard error of the mean is indicated as the error bars.

Sdq values until the end of the grinding process. Similarly to the observed trend for Sa (Fig. 9), the overall measured values for ABN800 appeared higher at lower volumes of material removed (>180 mm³) until a stable value is reached for ABN300.

3.4 Evolution of Functional Surface Texture Parameters.

Both the reduced peak height (Spk), which represents the average height of peaks above the core surface, and the peak material volume (Vmp) that represents the volume of the peaks at 10% material areal ratio, showed very high correlations with grinding duration. Both the Spk and Vmp values showed similar trends in evolution during point grinding, as shown in Fig. 12. While there is no initial drop-off in the measured value, such as observed for height-based parameters (e.g., Sa and Sp), the measured values decreased steadily throughout the grinding process, up to measurable critical values at Spk = 5.378 μm and Vmp = 0.254 ml/m², following prolonged grinding and the start of the bond engagement. It is also possible to observe that the average peaks for ABN800 are higher than ABN300 (Fig. 12(a)); however, their volumes throughout the tool life are similar (Fig. 12(b)).

Finally, considering both height-based and functional parameters, surface texture parameters that assess the void or valleys on the tool surface have also been evaluated. This subset of parameters, including the maximum valley depth (Sv), reduced valley height (Svk), and valley void volume (Vvv), consistently showed low values and significant differences between repeat tests resulting in large errors. The errors in each case were more extensive than the

measured changes as a result of wear though the life of the tool, even for the most severely worn surfaces.

4 Discussion

4.1 Surface Texture Parameter Ranking.

Depending on the nuances of any particular grinding process, different surface texture parameters can be used for monitoring the condition of the surface. In the case of small-scale point grinding, as discussed earlier, rapid wear of the tool surface and resultant limited total life is of concern. Therefore, it is crucial to detect the point at which the tool approaches the end of its useful grinding performance (the point of bond engagement). In this context, three key metrics have been used to evaluate the applicability of the measured surface texture parameters for monitoring the condition of the point grinding tool surface. The first two include the percentage change in the measured value and the correlation of the surface texture parameter with grinding duration, both of which have been used for a similar purpose in the past [11,18]. Additionally, the visibility of clear critical values upon bond engagement was used. These three key metrics allow the assessment of the magnitude and measurability of all investigated surface texture parameters, their relationship with wear and forces, and the ability to detect when the condition of the tool approaches failure, respectively. Based on the observed behaviors and trends, the performance of each surface texture parameter according to these three metrics has been assessed and recorded in Table 4, with scores from one to five assigned

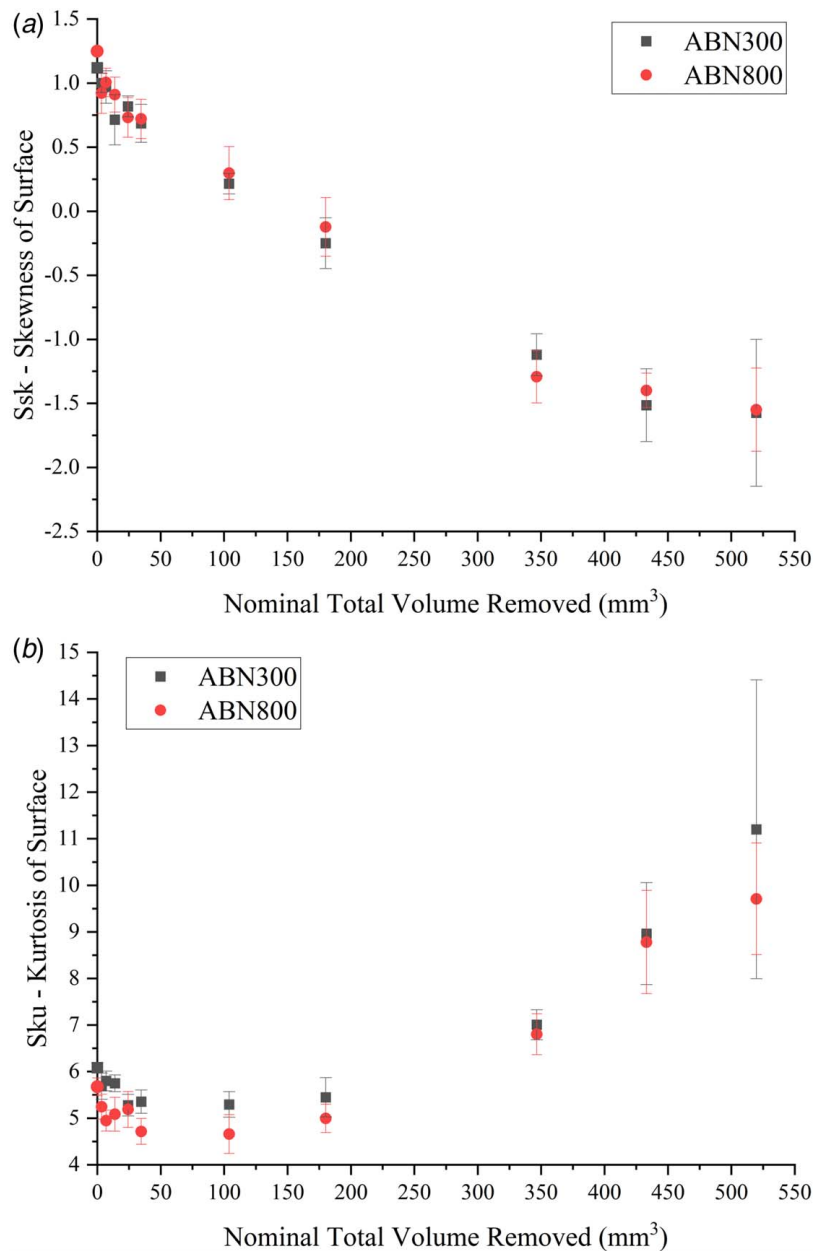


Fig. 10 Evolution of surface roughness (Ssk) and kurtosis (Sku) during point grinding. The standard error of the mean is indicated as the error bars.

between the lowest and highest values accordingly. Pearson and Spearman correlations [22] of each parameter with grinding duration were also calculated, with the best score used to assess the correlation with grinding duration. In summary, the parameters that focus on the peak portion of the material (e.g., Spk and Vmp) tend to show the most significant change during wear, while those evaluating the voids or valleys on the tool surface (e.g., Sv and Svv) showed the least change. Finally, some parameters showed obvious measurable threshold values when tool bond engagement occurred (e.g., Spk and Sdr), while others showed little to no change towards the end of tool life (e.g., Sz and Sv). Following the decision-matrix methodology, the individual scores were multiplied together, and the resulting final scores and rankings are shown in Table 4. Although the highly scoring parameters do not summarize the entire interaction and condition of the tool surface, these rapidly evolving and highly correlating surface texture properties can be monitored during grinding to evaluate the overall

condition of the point grinding tool and detect when the tool nears the end of its useful life. A more detailed discussion regarding the performance of these surface texture parameters, with a particular focus on the best scoring parameters, is presented next.

4.2 Best Performing Surface Texture Parameters. In order to aid the scoring and discussion of all the surface texture parameters, it is helpful to look at the arithmetic mean height of the surface (Sa) as a benchmark. This parameter calculates the absolute difference in the height of each point on the tool's surface from the arithmetical mean surface [20]. In the case of single-layer grinding tools, this is a useful measure of the average protrusion of the grains above the bond material. During the early stages of grinding, the Sa value decreases at a fast rate, up to the previously identified transition point around 34.65 mm³. This reflects the rapid wear-rate through fracturing, which has been previously identified as the dominant wear mechanism during this phase of wear [8]. As the grains on

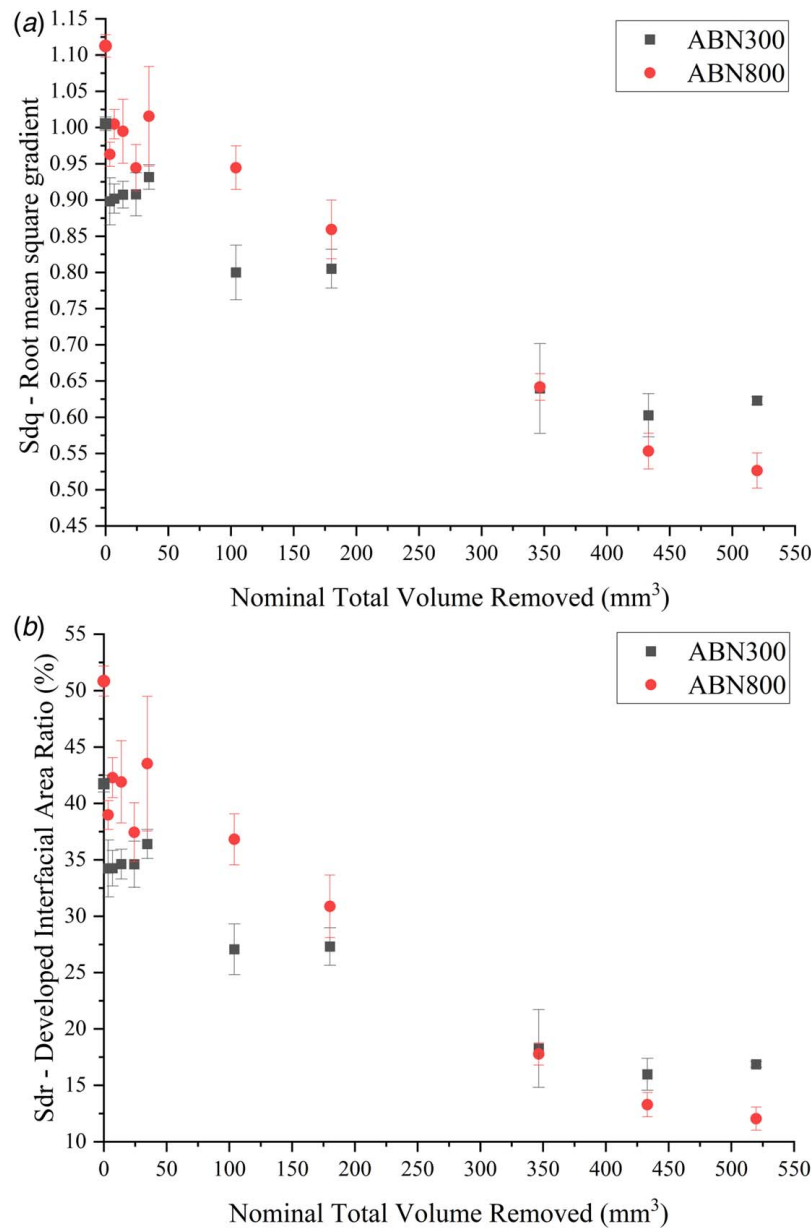


Fig. 11 Evolution of (a) root mean square gradient (Sdq) and (b) developed interfacial area ratio (Sdr) during point grinding. The standard error of the mean is indicated as the error bars.

the surface continue to wear through micro fracture, examples of them can be viewed on the grain surfaces in Fig. 7(a), the average height of the surface decreases with increasing grinding duration. Overall, when comparing the starting and end conditions of the Sa surface texture parameter value, a relatively large and measurable drop in surface height was observed, with low variation between repeat measurements and good correlation with grinding duration in comparison to other investigated surface texture parameters (as shown in Table 4). However, the Sa value did not reach zero even after the most prolonged cutting (519.75 mm³). Despite the bond layer being fully engaged, voids from missing or partially submerged grains remain below the mean reference plane. Therefore, the Sa = 0 μ m condition would only be approached when the bond material is completely stripped of the tool body. Finally, Sa measurements did not reveal any clear and easily measurable critical values for the identification of bond engagement. Instead, since the soft bond material can easily wear, the average height continued to decrease, with increased severity for ABN800.

From the subset of the six best performing surface texture parameters (Vmp, Spk, Ssk, Sdr, Sa, and Sdq), the reduced peak height (Spk), and the peak material volume (Vmp) scored significantly higher than the rest (Table 4). This result agrees with the earlier research by Barth [17] and Bazan [11], also suggesting that Vmp and Spk functional surface texture parameters evolve most with the wear of abrasive grains. In fact, the performance of these parameters has only been strengthened further by the addition of bond engagement assessment criteria in this investigation. An example of the calculation of such functional surface texture parameters is shown in Fig. 13. At the start of the grinding process, the grain protrusion is high (Fig. 6), and the corresponding heights (Fig. 13(a)) and volume of the peaks portion of the surface (Fig. 13(b)) is therefore also high. With the wear of the abrasive grains, a gradual reduction in the height and volume of this portion of the material is observed (Fig. 13(c)); however, unlike previously mentioned height parameters such as Sp, Sz, and S10z, these functional parameters are significantly less affected by debris and anomalies on the surface of the tool. There is, therefore, no initial rapid drop-off in

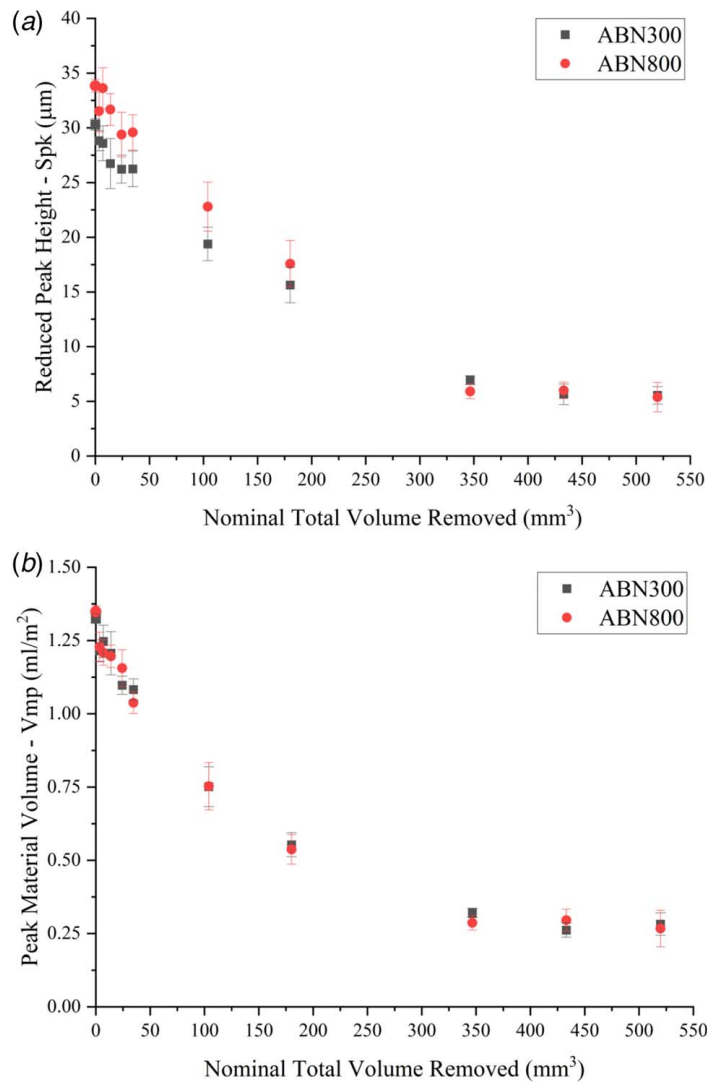


Fig. 12 Evolution of functional parameters reduced peak height (Spk) and peak material volume (Vmp) during point grinding. The standard error of the mean is indicated as the error bars.

Table 4 Individual scores and final ranking for most commonly used surface texture parameters

Surface texture parameters	ABN300			ABN800			% change	Correlation	Critical value	Total score	Rank
	Change	Pearson	Spearman	Change	Pearson	Spearman					
Height-based											
Sa	-45%	0.848	0.767	-62%	0.823	0.758	3	4	2	24	5
Sq	-46%	0.880	0.850	-60%	0.877	0.816	3	5	1	15	8
Sp	-57%	0.517	0.688	-71%	0.701	0.817	3	2	1	6	14
Sv	6%	0.043	0.055	-8%	0.202	0.196	1	1	1	1	17
Sz	-28%	0.511	0.599	-44%	0.613	0.668	2	2	1	4	15
S10z	-36%	0.694	0.778	-47%	0.811	0.802	2	3	1	6	13
Ssk	-238%	0.894	0.837	-218%	0.887	0.789	5	5	3	75	3
Sku	66%	0.644	0.259	63%	0.741	0.327	3	2	4	24	7
Hybrid											
Sdq	-39%	0.828	0.632	-51%	0.849	0.633	2	4	3	24	6
Sdr	-61%	0.812	0.653	-75%	0.800	0.659	4	3	4	48	4
Functional											
Sk	-29%	0.616	0.489	-53%	0.726	0.664	2	2	2	8	12
Spk	-82%	0.889	0.843	-83%	0.885	0.835	4	5	5	100	2
Svk	0%	0.019	0.113	2%	0.230	0.103	1	1	1	1	19
Smr1	-48%	0.865	0.613	-53%	0.697	0.529	3	2	2	12	11
Smr2	-3%	0.398	0.276	-7%	0.500	0.466	1	1	1	1	16
Vmp	-79%	0.889	0.900	-79%	0.880	0.894	4	5	5	100	1
Vmc	-38%	0.755	0.627	-59%	0.773	0.688	2	3	2	12	10
Vvc	-61%	0.807	0.673	-75%	0.778	0.676	4	3	1	12	9
Vvv	0%	0.034	0.073	-6%	0.299	0.150	1	1	1	1	18

Note: The six highest ranking parameters are highlighted in bold.

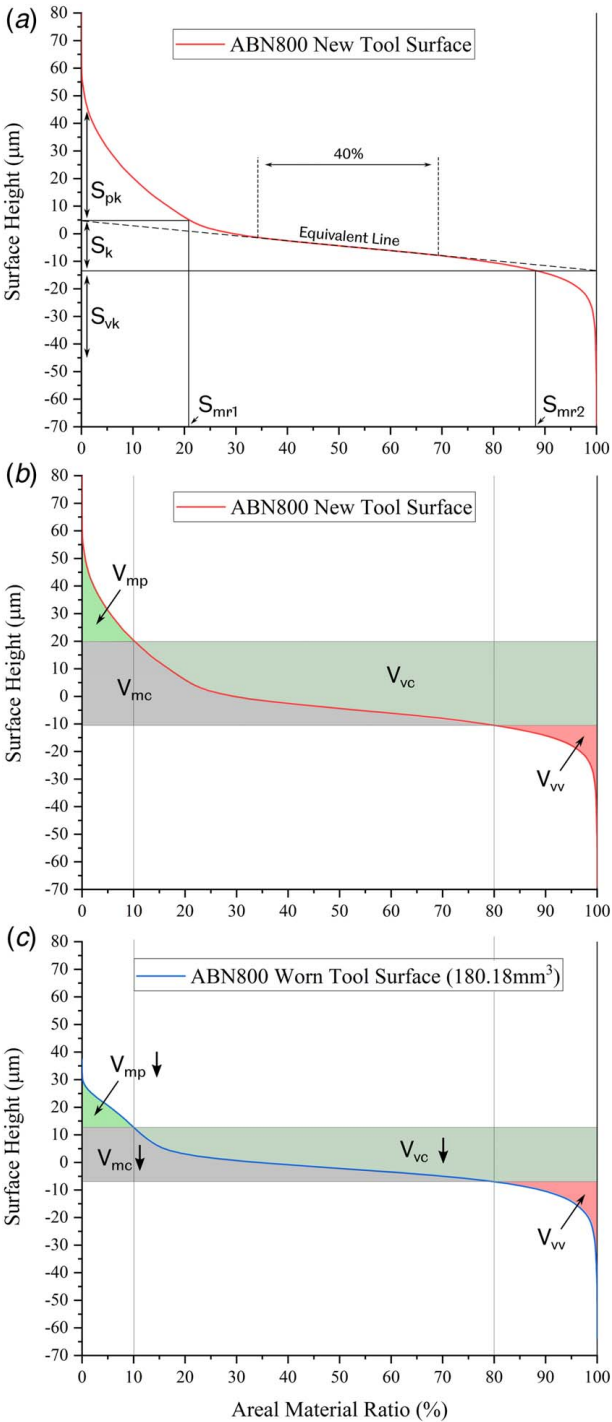


Fig. 13 Calculation of functional parameters based on heights (a) and volumes (b, c), (b) comparison of new tool surface, and (c) worn surface parameters after 180.18 mm³ of material removed

value during the first grinding passes, and much-reduced errors in the case of S_{pk} and V_{mp} , for assessing the overall height and volume of the active abrasive grains.

While in the case of height-based parameters, following bond engagement, the value continues to decrease, both S_{pk} and V_{mp} remained stable up to the end of the experiment after reaching a critical value once bond engagement has occurred. Most likely, the remaining height ($S_{pk} = 5.378 \mu\text{m}$) and volume per unit area (0.254 ml/m^2) represent the peaks of the texture remaining on the bond material from rubbing with the workpiece (Fig. 14).

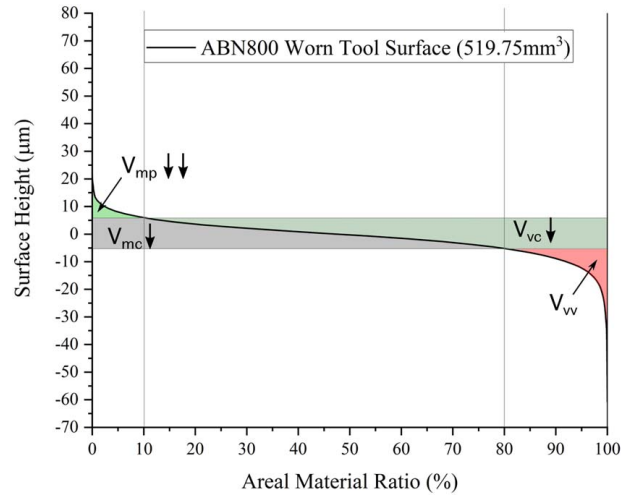


Fig. 14 Functional volume parameters of a severely worn ABN800 surface after 519.75 mm³ of material removed

The surface skewness (S_{sk}) and kurtosis (S_{ku}) values, which consider the skew and sharpness of the distribution of the measured surface heights, respectively, have also scored relatively high compared to other surface texture parameters. The relatively high ranking of the S_{sk} parameter was previously reported by Bazan [11], and in this investigation showed the highest correlation with grinding duration out of all measured texture parameters. This resulted in the good overall performance of the parameter for tool condition monitoring, with the third-highest total score (Table 4), as it was only negatively impacted by the absence of clear critical values upon bond engagement. The tool surface kurtosis (S_{ku}) values, on the other hand, have not received any special mention [17,18] or have been completely omitted [11] in earlier research. To understand the evolution of both these parameters, it is useful to look closer at the distribution of the surface heights at various stages of wear (Fig. 15). From a new condition tool surface, as the most protruding grains partially wear down, a second peak in the distribution can be seen forming around $22 \mu\text{m}$, resulting in a decrease of the surface Kurtosis value and change in skewness towards zero. As more grains become active and wear progress beyond the second peak, the kurtosis value of the tool surface begins to increase, as one high peak in the distribution is formed,

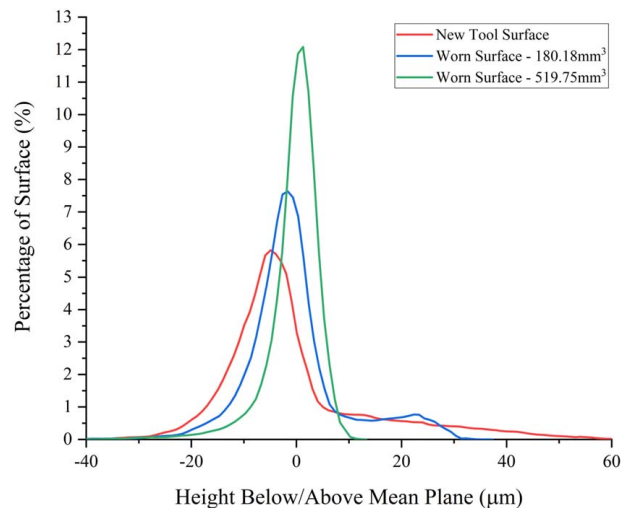


Fig. 15 Typical evolution of the point grinding tool surface height distribution

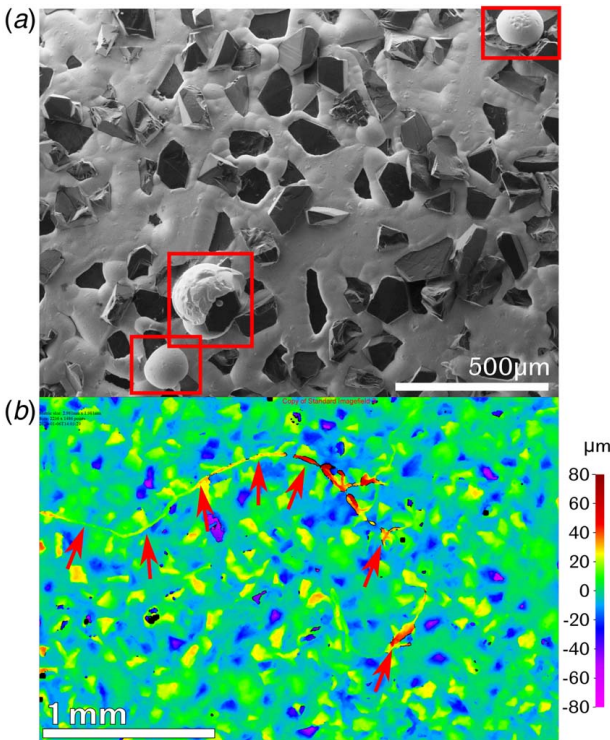


Fig. 16 (a) Secondary electron SEM image of new condition ABN800 tool surface with highlighted highly protruding bond nodules above the abrasive grains and (b) worn ABN300 3D surface contaminated with fiber following grinding test

and the S_{sk} value shifts to negative values. Furthermore, as bond engagement occurs, a rapid increase in S_{ku} is observed. While no specific critical value was identified during bond engagement for either parameter (Fig. 10), the evolution of kurtosis could be monitored during grinding, with a positive gradient in its evolution indicating degradation of the tool surface.

Finally, both the surface developed interfacial area ratio (S_{dr}) and root mean square gradient (S_{dq}) also performed well for the assessment of tool condition during grinding (Table 4). Unlike most other height-based and functional parameters, however, these hybrid parameters showed an additional peak in their evolution at the transition point from the initial rapid wear to stable grinding (around 34.65 mm^3), as shown in Fig. 4 previously. This minor peak could result from fracture wear creating additional texture and gradients on the grains during the initial transient wear stage [7]. This peak in the evolution of the surface texture parameter was unique to S_{dr} and S_{dq} , and previously unreported, and could potentially be used to identify the transition point to steady grinding during on-machine monitoring of the tool condition. Following this transition point, as micro fracturing and wear flat formation become the dominant wear mechanisms leading to the flattening of the grain tips, the S_{dr} and S_{dq} values continue to fall. For a perfectly planar surface, both parameters will have a zero value, while any additional surfaces or gradients contributed by texture will result in higher values [20]. In the case of single-layer wheels, therefore, both hybrid parameters are expected to tend towards zero as the tool continues to wear and bond engagement eventually occurs; however, the zero point was not reached during the tested grinding durations (Fig. 11). Similarly to the overall height of the surface (S_a), the presence of voids below the plating layer height produced additional texture that is greater than that of a planar surface, resulting in an increase in the measured values above zero. Due to their similarity, both parameters appear to evolve identically with increased volume of material removed, showing a good correlation with grinding duration. In addition, as the measured values are not

relative to the mean plane or bond level, the measurements were not affected by variation of the bond level, and the overall errors between repeat measurements were therefore low, giving both these parameters a high score.

4.3 Poorly Performing Surface Texture Parameters.

Amongst the six lowest-scoring parameters, four focused on the voids or valleys of the tool surface (S_v , S_{vk} , S_{mr2} , and V_{vv}). A similar observation was also made by Bazan [11], where V_{vv} and S_v were reported amongst the lowest ranking parameters. These parameters, in most cases, did not evolve measurably with wear and, therefore, showed the lowest correlations with grinding duration. This behavior can be expected in these point grinding tools due to the very low number of grains worn by pullout. The portions of material considering the valley depths and volumes remain largely unchanged even after bond engagement occurs (Figs. 13 and 14). However, it is important to note that for another single-layer tooling that may contain weaker bonded grains, these parameters could become critical to quantify the extent of pullout (e.g. void volume: V_{vv}).

It was previously mentioned that maximum peak height (S_p) and maximum peak to valley height (S_z) showed relatively large errors between repeat tests (Fig. 9). This was mainly due to the presence of occasional anomalies during imaging, such as bond nodules before grinding and dust and debris on the surface of the tool after grinding, which resulted in occasional abnormally high peaks on the measured tool surface. Example tool surfaces containing such features are shown in Fig. 16. As the imaging was performed on tools following only minor cleaning to simulate on-machine conditions, such occasional defects are unavoidable and are essential to account for in the practical application of any imaging technique. These anomalies were most notable for S_p and S_z , which are considered the highest points on the tool surface but also negatively affected other height-based surface texture parameters.

4.4 Uneven Wear Around Tool Circumference.

As mentioned earlier, there also appeared to be a variation in the surface condition around different sides of the same point grinding tools (Fig. 6). Under closer inspection using surface texture parameters, this becomes even clearer. Figures 17(a) and 17(b) show the evolution of the peak material volume (V_{mp}) for both abrasive grades across the three different sides of each tool. As can be expected, the volume of peaks lost to wear increased progressively with the increasing volume of material removed; however, it can also be seen that the volume of the CBN grains lost is non-uniform around different sides of the tool. In some instances, sides containing the largest gain volumes lost the most material (ABN300: 6.93 mm^3), while in other cases, the opposite was true (ABN800: 24.255 mm^3). A similar pattern was observed for the other key surface texture parameters. This behavior could possibly be explained by an underlying issue such as tool runout affecting the results. However, it is unclear precisely what the critical factor in controlling this behavior is, and further investigations of this behavior are needed to fully understand and improve the performance of these tools.

4.5 Parameter Suitability for Condition Monitoring.

As stated earlier, this investigation aimed to identify the most significant parameters for monitoring the condition of single-layer cBN point grinding tools and address a key gap in understanding their evolution over time. By observing the trends in the evolution of the surface texture parameters, additional insight into the condition of the grinding wheel has been obtained, which would otherwise be missed if only considering fixed points in the life of the point grinding tool. The discussion so far focused on the ability of the surface texture parameter to assess the overall condition of the surface, and detect bond engagement, with the aim of assessing the remaining tool life and ensuring safe and reliable performance. For that

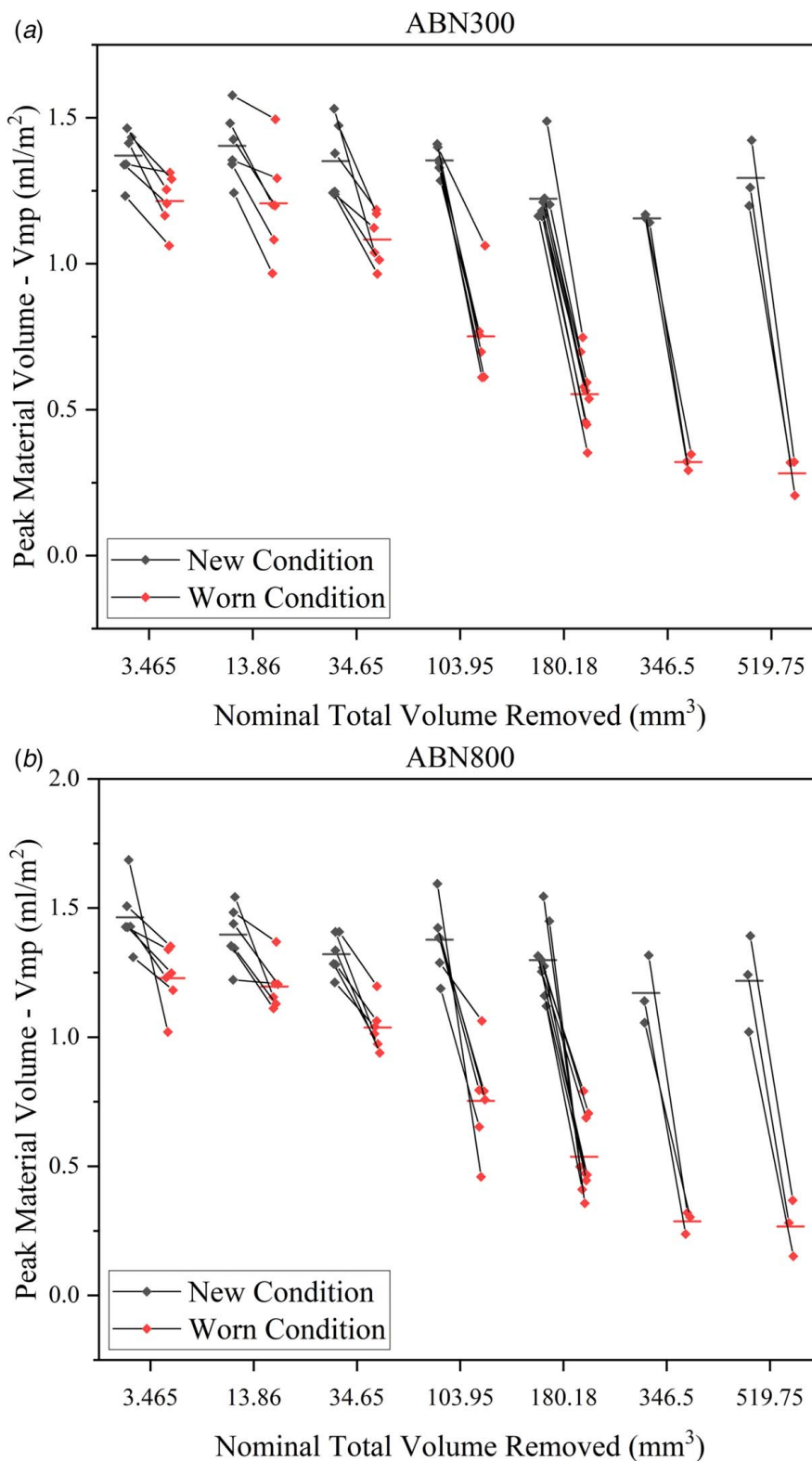


Fig. 17 Comparison of matching new and worn condition surface peak material volumes (Vmp) from three sides of the same tool following point grinding using (a) ABN300 and (b) ABN800 abrasive under various durations

purpose, the obtained results confirm the observations by Barth [17] and Bazan [11], identifying Vmp and Spk as the best performing parameters. However, the results also show that no one fits all parameter exists, and if the aim or purpose of the condition monitoring process was to change, the best parameter set could also change.

Fully understanding the trends in the evolution of the point grinding tool surface texture parameters now allows the selection of an appropriate parameter set based on the need of the process or inspection. Some further examples of this are shown in Table 5.

Table 5 Recommended grinding wheel surface texture parameters for various condition monitoring scenarios

Scenario	Aim/Purpose	Best parameters
Assessment of overall surface condition	Estimate grinding potential and remaining tool life	Vmp, Spk, and Ssk
Detect stable grinding transition point	Inform tool run-in duration to ensure reliable performance	Sdr and Sdq
Detect bond engagement	Forecast end of tool life and prevent failure	Vmp, Spk, Sdr, and Sku
Quantify grain pullout	Estimate bonding strength and reduce grain loss	Vvv and Svk

5 Conclusion

The evolution of point grinding tool surface over time with respect to height-based, hybrid, and functional surface texture parameters has been investigated. From the 19 most commonly used surface texture parameters, average surface height (Sa), skewness (Ssk), root mean square gradient (Sdq), developed interfacial area ratio (Sdr), reduced peak height (Spk), and peak material volume (Vmp) all showed the highest correlation with wear and grinding duration of electroplated cBN point grinding tool surfaces. Furthermore, from this subset of highly performing surface texture parameters, Spk and Vmp showed the best results for monitoring the condition of single-layer point grinding tools, with a high correlation against grinding duration and the ability to identify bond engagement through the presence of critical values. On the other hand, due to the limited amount of wear by grain pullout, the texture parameters that consider the voids or valleys on the tool's surface showed the lowest overall performance scores. These included maximum valley depth (Sv), reduced valley height (Svk), and valley void volume (Vvv). This investigation also demonstrated the possibility of direct measurement of the grinding wheel surface (without the creation of replicas) and examined its influence on the measured surface texture parameters errors, which is a key step in enabling the on-machine application of focus-variation measurement for future work. And finally, the measured surface wear was found to be highly uneven around the circumference of the point grinding tools. While it is likely due to runout and variation in bond and grain protrusion heights, future work will be needed to fully understand this behavior further.

Acknowledgment

This research was supported by Rolls Royce plc., Element 6, and EPSRC (Grant EP/L016257/1).

Conflict of Interest

There are no conflicts of interest.

Data Availability Statement

The datasets generated and supporting the findings of this article are obtainable from the corresponding author upon reasonable request.

Nomenclature

a = depth of cut, mm
 v_s = cutting speed, m/s
 v_w = feed rate, mm/min
cBN = cubic boron nitride
Sa = average height of surface, μm
Sdq = root mean square gradient

Sdr = developed interfacial area ratio, %
Sk = core roughness depth, μm
Sku = kurtosis of surface heights distribution
Smr1 = peak material component, %
Smr2 = valley material component, %
Sp = maximum peak height, μm
Spk = reduced peak height, μm
Sq = root mean square height of surface, μm
Ssk = skewness of surface heights distribution
Sv = maximum valley depth, μm
Svk = reduced valley depth, μm
Sz = maximum height, μm
S10z = ten-point height, μm
Vmc = core material volume, ml/m^2
Vmp = peak material volume, ml/m^2
Vvc = core void volume, ml/m^2
Vvv = valley void volume, ml/m^2

References

- [1] Malkin, S., and Guo, C., 2008, *Grinding Technology: Theory and Application of Machining with Abrasives*, Industrial Press Inc., New York, pp. 1–33.
- [2] Rowe, B., 2014, *Principles of Modern Grinding Technology*, Elsevier, Oxford, pp. 35–58.
- [3] Ding, W., Linke, B., Zhu, Y., Li, Z., Fu, Y., Su, H., and Xu, J., 2017, "Review on Monolayer CBN Superabrasive Wheels for Grinding Metallic Materials," *Chinese J. Aeronaut.*, **30**(1), pp. 109–134.
- [4] Aspinwall, D. K., Soo, S. L., Curtis, D. T., and Mantle, A. L., 2007, "Profiled Superabrasive Grinding Wheels for the Machining of a Nickel Based Superalloy," *CIRP Ann.—Manuf. Technol.*, **56**(1), pp. 335–338.
- [5] Curtis, D. T., Soo, S. L., Aspinwall, D. K., and Mantle, A. L., 2016, "Evaluation of Workpiece Surface Integrity Following Point Grinding of Advanced Titanium and Nickel Based Alloys," *Procedia CIRP*, **45**, pp. 47–50.
- [6] Pietrow, N., Curtis, D., Ghadbeigi, H., Novovic, D., and McGourlay, J., 2021, "An Investigation Into the Challenges of the Point Grinding Machining Process," *Procedia CIRP*, **101**, pp. 190–193.
- [7] Shi, Z., and Malkin, S., 2006, "Wear of Electroplated CBN Grinding Wheels," *ASME J. Manuf. Sci. Eng.*, **128**(1), pp. 110–118.
- [8] Guo, C., Shi, Z., Attia, H., and McIntosh, D., 2007, "Power and Wheel Wear for Grinding Nickel Alloy With Plated CBN Wheels," *CIRP Ann.—Manuf. Technol.*, **56**(1), pp. 343–346.
- [9] Yu, T., Bastawros, A. F., and Chandra, A., 2017, "Experimental and Modeling Characterization of Wear and Life Expectancy of Electroplated CBN Grinding Wheels," *Int. J. Mach. Tools Manuf.*, **121**, pp. 70–80.
- [10] Shi, Z., and Malkin, S., 2003, "An Investigation of Grinding With Electroplated CBN Wheels," *CIRP Ann.*, **52**(1), pp. 267–270.
- [11] Bazan, A., Kawalec, A., Ryzak, T., and Kubik, P., 2020, "Variation of Grain Height Characteristics of Electroplated cBN Grinding-Wheel Active Surfaces Associated With Their Wear," *Metals*, **10**(11), pp. 1–18.
- [12] Hood, R., Medina Aguirre, F., Soriano Gonzalez, L., Novovic, D., and Soo, S. L., 2019, "Evaluation of Superabrasive Grinding Points for the Machining of Hardened Steel," *CIRP Ann.*, **68**(1), pp. 329–332.
- [13] Blunt, L., and Ebdon, S., 1996, "The Application of Three-Dimensional Surface Measurement Techniques to Characterizing Grinding Wheel Topography," *Int. J. Mach. Tools Manuf.*, **36**(11), pp. 1207–1226.
- [14] Tönshoff, H. K., Friemuth, T., and Becker, J. C., 2002, "Process Monitoring in Grinding," *CIRP Ann.—Manuf. Technol.*, **51**(2), pp. 551–571.
- [15] Cai, R., Rowe, W. B., Morgan, M. N., and Mills, B., 2003, "Measurement of Vitrified CBN Grinding Wheel Topography," *Key Eng. Mater.*, **239**, pp. 301–306.
- [16] Puerto, P., Kirsch, B., Madariaga, J., Fernández, R., Aurich, J. C., and Gallego, I., 2015, "A Comparison of Techniques to Measure the Wear Flat Area of Conventional and Superabrasive Grinding Wheels," *ASME J. Tribol.*, **137**(2), p. 024503.
- [17] Barth, S., and Klocke, F., 2017, "Influence of the Grinding Wheel Topography on the Thermo-Mechanical Stress Collective in Grinding," *Inventions*, **2**(4), p. 34.
- [18] Kacalak, W., Lipiński, D., Szafraniec, F., and Tandecka, K., 2018, "The Methodology of the Grinding Wheel Active Surface Evaluation in the Aspect of Their Machining Potential," *Mechanik*, **91**(8–9), pp. 690–697.
- [19] Franco, L. A., and Sinatora, A., 2015, "3D Surface Parameters (ISO 25178-2): Actual Meaning of Spk and Its Relationship to Vmp," *Precis. Eng.*, **40**, pp. 106–111.
- [20] ISO, 2012, "ISO 25178-2 Geometrical Product Specifications (GPS)—Surface Texture: Areal—Part 2: Terms, Definitions and Surface Texture Parameters".
- [21] ISO, 2014, "ISO 16610-71 Geometrical Product Specifications (GPS)—Filtration—Part 71: Robust Areal Filters: Gaussian Regression Filters".
- [22] Weaver, K. F., Morales, V., Dunn, S. L., Godde, K., and Weaver, P. F., 2017, "Pearson's and Spearman's Correlation," *An Introduction to Statistical Analysis in Research*, John Wiley & Sons, Inc., Hoboken, NJ, pp. 435–471.